

11 Supersonic base flow

A. Garbaruk, M. Shur, M. Strelets, A. Travin (NTS)

11.1 Introduction

A supersonic flow downstream of a blunt-based cylinder is characterized by a very complicated vortical structure of the base near wake, which includes a separated shear layer, recirculation zone, recompression region, and trailing wake subjected to strong compressibility effects. Other than that, the geometry is axisymmetric, which makes its computation more difficult in terms of both turbulence representation and numerics. Finally, this kind of flow is commonly found behind such objects as missiles, rockets, and projectiles, and the low pressure behind the base causing “base drag” can be a sizable portion of the total drag. Thus, a capability of a turbulence model to predict the base pressure accurately is of significant practical importance. For these reasons, experimental data on such a flow obtained in the study of Herrin and Dutton (1994) present an attractive database for validation of innovative turbulence simulation approaches. All these and, also, availability of the experimental data in a digital form motivated including this flow in the list of DESider test cases.

11.2 Test case presentation

The flow is a near wake of a circular cylinder with adiabatic walls aligned with a uniform supersonic flow (see sketch in Fig.1). The flow parameters the experiments of Herrin and Dutton were performed at are presented in Table 1.

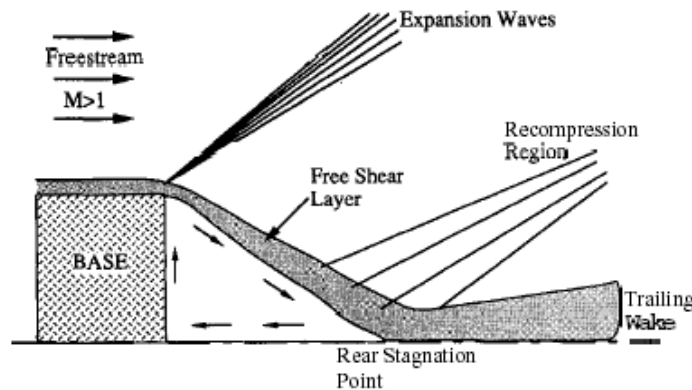


Figure 1 Schematic of supersonic flow in near wake of the cylinder

The flow quantities measured in the experiment and available for a comparison with results of computations include a radial distribution of static pressure over the

cylinder base, $C_p(r)$, and velocity, Mach number, and Reynolds shear stress fields in the near wake.

Table 1 Major parameters of Herrin and Dutton (1994) experiment

Parameter	Notation	Value
Reynolds number	$Re=U_\infty R/\nu$	1.632×10^6
Cylinder radius	R	0.03175 m
Free stream Mach number	M	2.46
Stagnation Temperature	T_s	293 K
Free stream velocity	U_∞	564.2 m/s
Free stream temperature	T_∞	131 K

11.3 Participants and methods used

A list of the partners who computed this flow and key-information on turbulence modelling approaches, numerical methods, and computational grids they used are presented in Table 2, whereas Figs.2-5 give an idea on the grids topology and computational domains used in the simulations.

Table 2 Summary of simulations

Partner	Model	Numerics		Grid size and type	Time Step/Sample
		Space	Time		
DLR	S-A DES	AUSMDV	LUSGS	3.6 Million, structured (NTS)	0.0935/37
FOI	S-A RANS	2nd ctr.	Impl.	0.9 Million, unstructured (DLR)	Steady
	S-A DES		2nd Impl.		0.045/375
	HYB0				1.8 Million, structured (FOI)
NTS	S-A RANS	3rd upw.	Impl.	1.8 Million, structured (NTS)	Steady
	S-A RANS with Compressibility Correction				Steady
	S-A DES	3rd upw./ 4th ctr.	2nd Impl.	1.8 Million, structured (NTS)	0.01/200
	S-A DES				3.6 Million, structured (NTS)
ONERA	Zonal S-A DES (CDES=0.40)	AUSM+(P)	2nd Gear	14 Million, structured (ONERA)	0.018/n.a.

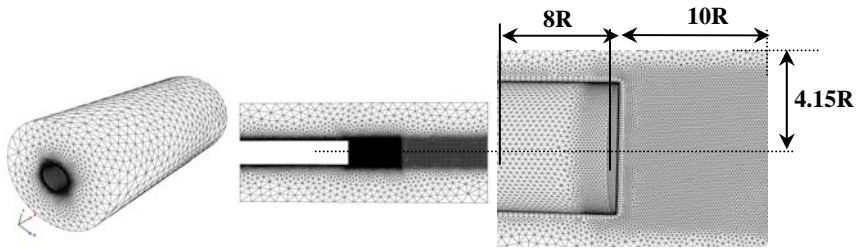


Figure 2 DLR unstructured grid, 0.9 M nodes, 18 prismatic layers near the surface.
Computational domain: $L_x=(8R + 10R)$, $L_t = 4.15R$

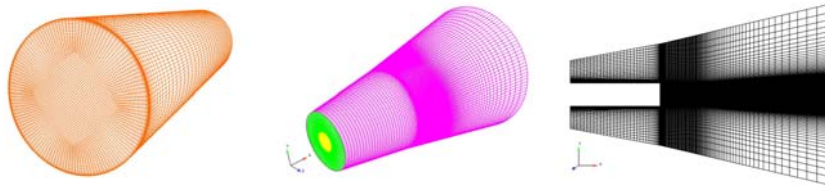


Figure 3 FOI structured grid, 1.8 M nodes. Computational domain: $L_x=(8R+15R)$,
 $L_t=(3-8)R$

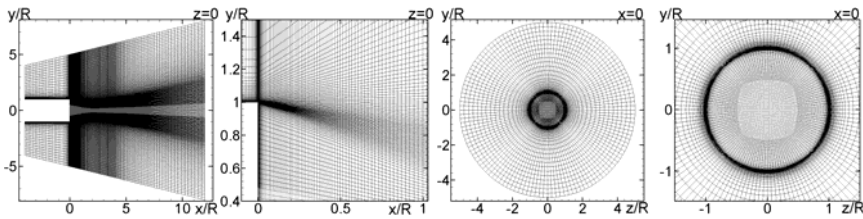


Figure 4 NTS multi-block structured grids: coarse 1.8 M nodes; fine 3.6 M nodes.
Computational domain: $L_x=(4R+12R)$, $L_t=(4-8)R$. $N_\phi=128$ in the outer block of the fine grid
and 96 in the coarse one

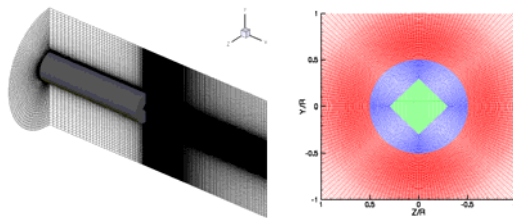


Figure 5 ONERA structured multi-block grid, 14 M nodes. Computational domain:
 $L_x=(8R+10R)$, $L_t=4.15R$. $N_\phi=180$

The inflow boundary conditions include imposing streamwise velocity profile. In the simulations it has been adjusted to match available experimental profile at $x/R = -0.0315$. Figure 6 shows to what extent different partners have reached this. One can see that in the simulation of FOI the inlet velocity profile noticeably deviates from the data. This should be kept in mind when analyzing results of the simulations presented below.

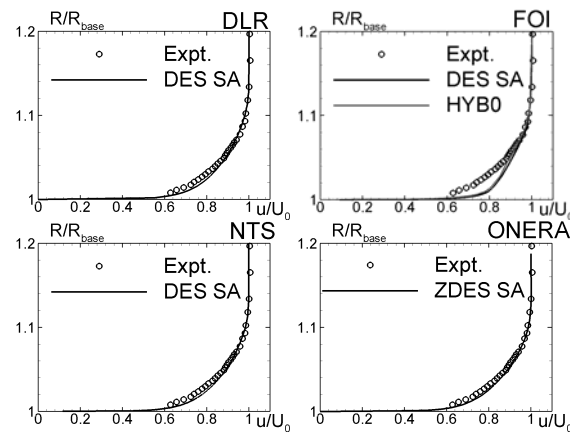


Figure 6 Computed and experimental velocity profiles at $x/R = -0.0315$

11.4 Results and discussion

11.4.1 RANS solutions

RANS computations of the flow were carried out by FOI and NTS with the use of the standard S-A model. In addition, NTS performed a computation with the use of the S-A model with the compressibility correction of Spalart (2000). Obtained RANS solutions are used as a baseline for evaluation of the turbulence-resolving approaches, since they permit to find out whether these, much more computationally expensive, approaches really overpass RANS-based modelling of the considered flow in terms of accuracy.

Figure 7 compares all the three solutions with each other and with the experimental data. It suggests that, despite somewhat different inlet velocity profiles (see Fig.6), results obtained by FOI and NTS with the use of the standard S-A model are close to each other, thus supporting a credibility of the model implementation in both flow solvers. Other than that, the figure clearly demonstrates a positive effect of the compressibility correction (dashed lines in the figure). However, even with this correction, the agreement of the RANS predictions with the data remains far from perfect, especially as far as the base-pressure is concerned: unlike virtually constant C_p in the experiment, RANS predicts a “wavy” C_p profile deviating from the data by up to 25%, which is

typical of all the RANS computations of the massively separated flows over bluff bodies.

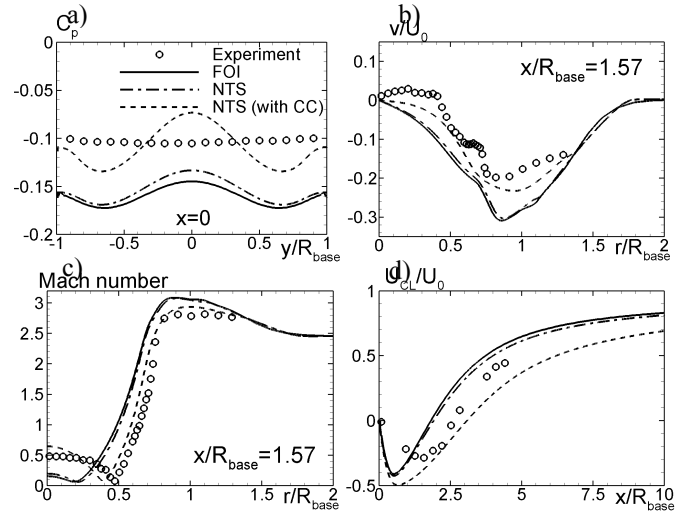


Figure 7 RANS solutions obtained with different models and codes. (a): radial pressure distribution at the cylinder base; (b) and (c): radial velocity and Mach number profiles in the near wake; (d): streamwise velocity distribution along the wake centreline

11.4.2 Turbulence-resolving simulations

These simulations were carried out with the use of three approaches (see Table 2): the standard S-A DES (DLR, FOI, NTS), zonal S-A DES of Deck (2005), (ONERA), and an algebraic hybrid RANS-LES model HYB0 of Peng (2005), (FOI).

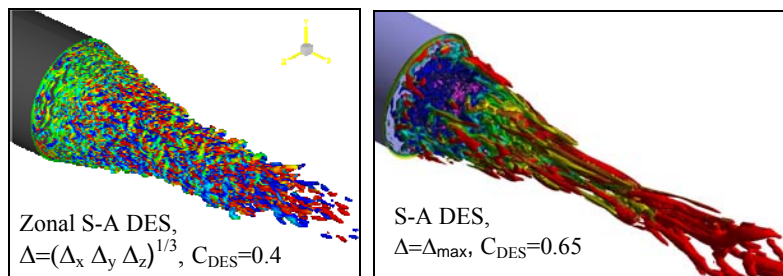


Figure 8 Flow visualizations from zonal S-A DES of ONERA and S-A DES of NTS (fine NTS grid)

Figure 8 compares resolved turbulence structures from the zonal DES of ONERA (Simon et al., 2006) and the S-A DES of NTS. One can see that both approaches provide for a realistic representation of the complex vortical structure of the considered flow. At the same time, it clearly demonstrates that a very fine grid used by ONERA provides for a resolution of much smaller eddies in the separated shear layer, thus suggesting a severe need for a fine grid in this flow region. Note, however, that the resolution of the finer structures in the zonal DES is partially reached due the use of the cube root of the cell size and a smaller C_{DES} constant (0.4 versus 0.65) for the sub-grid scale in the LES zone, which, arguably, may cause some inaccuracy of turbulence representation.

A common feature of DLR, FOI, and NTS simulations is that they suffer from some asymmetry of the mean flow. This is seen in Fig.9, where the contours of the time-averaged streamwise velocity at two wake's sections are presented from the NTS coarse and fine grid simulations. The figure shows also that a restricted grid-refinement (2 times increase of the total nodes count) almost does not diminish the asymmetry. However, the simulation of ONERA with the much finer grid in the shear layer produces a virtually symmetric mean flow. Thus, exactly the insufficient resolution of the shear layer is responsible for the asymmetry of the DLR, FOI, and NTS mean flow predictions. Unfortunately, this asymmetry virtually rules out a consistent comparison of the mean flow calculations with the use of different approaches without averaging of the solutions over the azimuthal direction ϕ . This circumstance had not been foreseen in the beginning of the work, and so not all the partners saved the information needed for the averaging in the course of their simulations. For this reason, in the following discussion, if ϕ -averaged fields are not available, we are forced to present sectional fields.

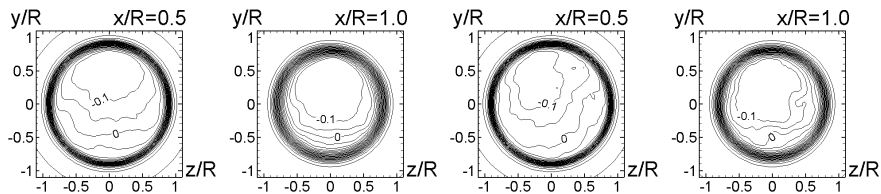


Figure 9 Time-averaged streamwise velocity u/U_0 from NTS S-A DES on coarse (two left frames) and fine (two right frames) grids

The rest figures give an idea on the effect of modelling approach, grid, and numerics on the quality of obtained solutions and their agreement with experiment.

Figure 10 shows the instantaneous vorticity fields from all the simulations. It suggests that independently of the modelling approach (either S-A DES or HYB0) the coarse unstructured DLR grid with 0.9 million nodes does not resolve any fine turbulent structures. With the fine NTS grid (3.6 million nodes), both DLR and NTS flow solvers permit to resolve much finer vortical structures, but NTS numerics is less dissipative. Same comment is true with regard to the FOI solver: the resolution it provides on the FOI structured grid, which is very close to the

NTS coarse one, is quite a bit worse than that provided by the NTS solver. These findings are quite consistent with the expectations based on the general notion on the reaction of any turbulence-resolving approaches to a grid-refinement and lowering of numerical dissipation.

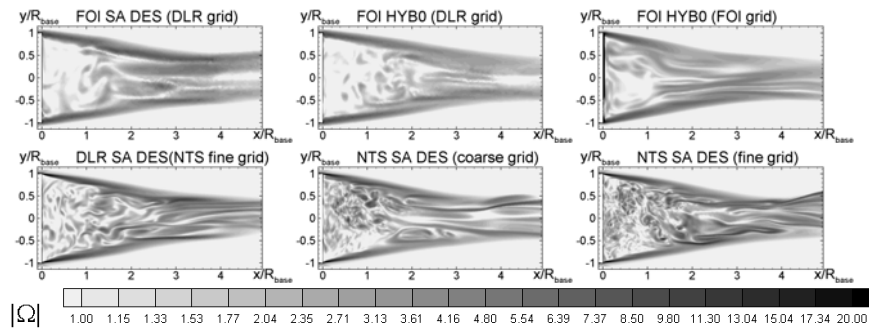


Figure 10 Effect of modelling approach, numerics (flow solver), and grid on the instantaneous vorticity field

Figures 11-13 compare time-averaged solutions obtained with the use of the different modelling approaches, flow-solvers, and grids. Upper parts of the frames in these figures show the experimental data and lower parts present results of the simulations.

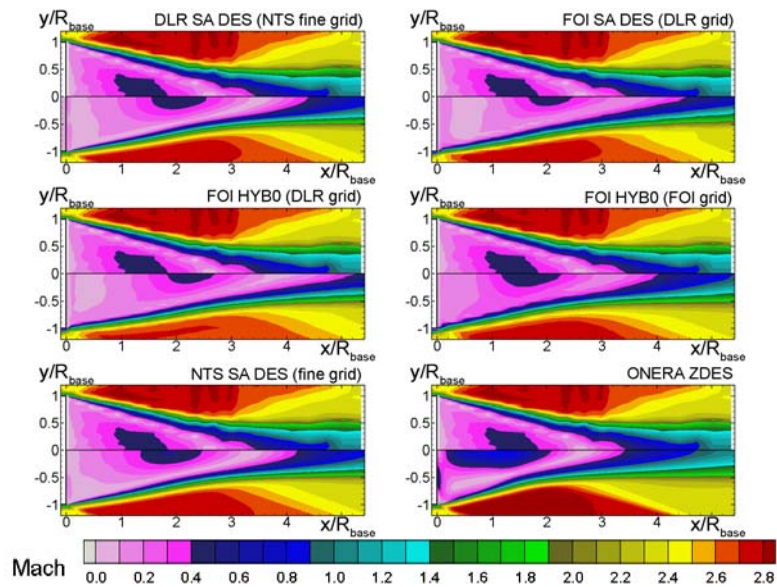


Figure 11 Mean Mach number in meridian plane

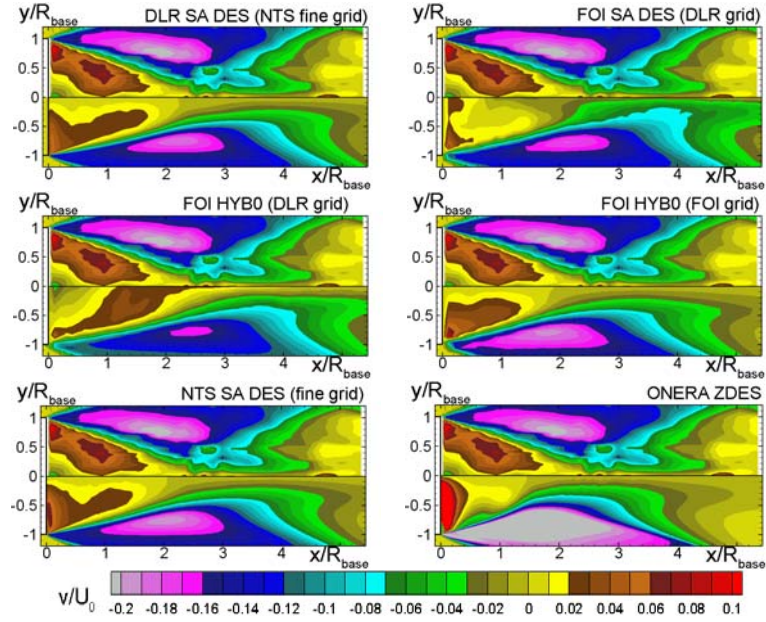


Figure 12 Mean radial velocity in meridional plane

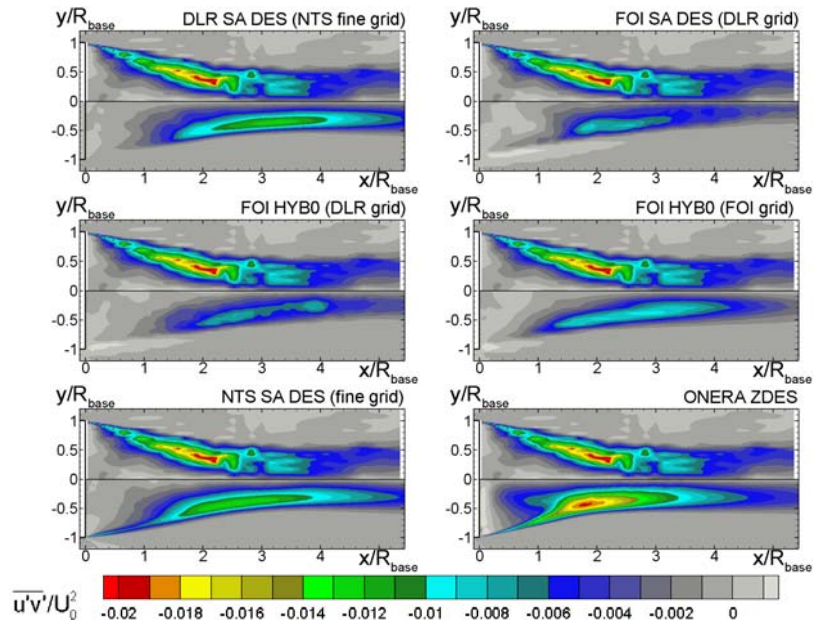


Figure 13 Full (resolved plus modelled) shear stress in meridional plane

Major conclusions that can be drawn based on the analysis of the results presented in the figures are as follows.

First, all the simulations, except for the ONERA one carried out with the use of the very fine grid in the shear layer, significantly overestimate the length of the recirculation zone (Fig.11) and underestimate the shear stress in the shear layer (Fig.13). The fine grid of NTS helps to weaken this flaw to some extent but obviously is still not sufficient.

Second, as expected based on the flow visualizations in Fig.10, the coarse unstructured DLR grid fails to provide a correct prediction of the flow independently of the modelling approach (either S-A DES or HYB0), whereas both the fine and coarse (not shown) NTS grids and the structured grid of FOI (as already mentioned, it is close to the coarse NTS grid) provide quite an acceptable representation of all the flow features, except for the length of the recirculation zone and shear stress in the initial region of the shear layer. On the other hand, despite the very fine grid, the zonal S-A DES of ONERA results in rather inaccurate prediction of the flow *inside* the recirculation zone (Figs.11-13).

These observations are quantitatively supported by Figs.14-16. In particular, Fig.14 shows that the mean flow characteristics computed by NTS on its coarse and fine grids are very close to each other. As has been already noted, this does not mean, of course, that even the coarse grid is sufficient for an overall (including the initial region of the shear layer) grid-independent solution: just neither the coarse nor the fine NTS grid provides for a sufficient resolution of this region.

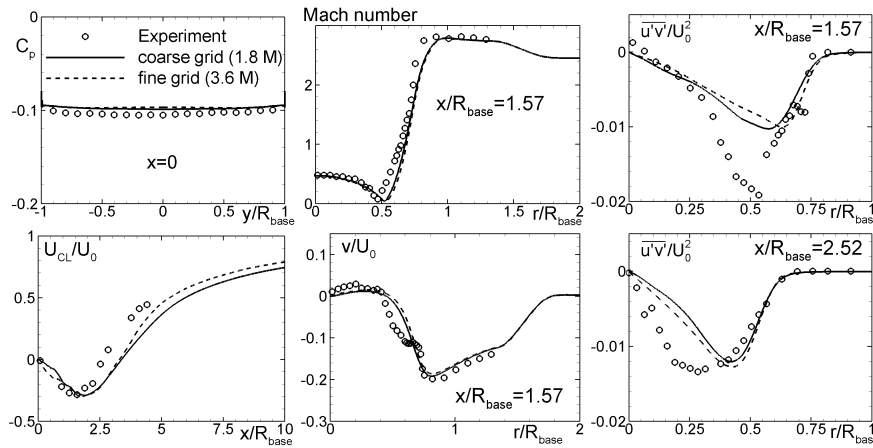


Figure 14 Effect of grid on S-A DES prediction of ϕ -averaged mean flow (NTS results)

Figure 15 compares HYB0 mean solutions obtained on the coarse unstructured DLR grid with that on the structured grid of FOI. Consistently with the above conclusion regarding the inability of the DLR grid to provide accurate turbulence representation, it turns out that it is insufficient for the mean flow prediction either. In contrast to this, with a finer grid, HYB0 performs reasonably well,

except for the prediction of the shear stress in the shear layer where, as already mentioned, a much finer resolution is needed.

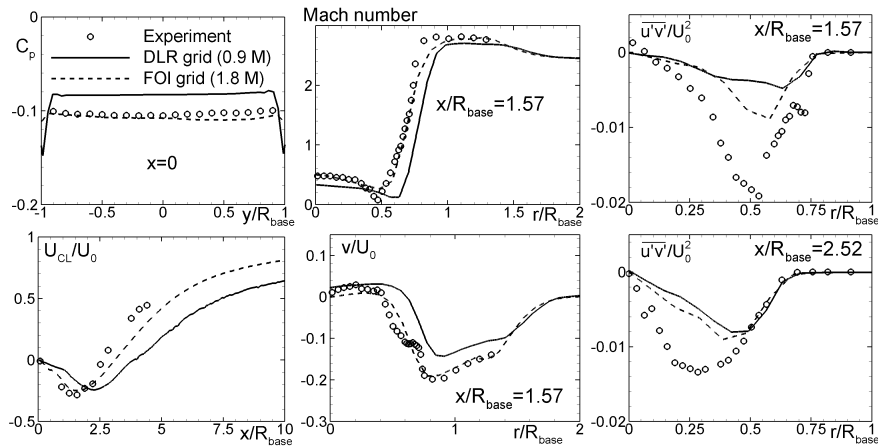


Figure 15 Effect of grid on HYB0 prediction of the ϕ -averaged mean flow (FOI results)

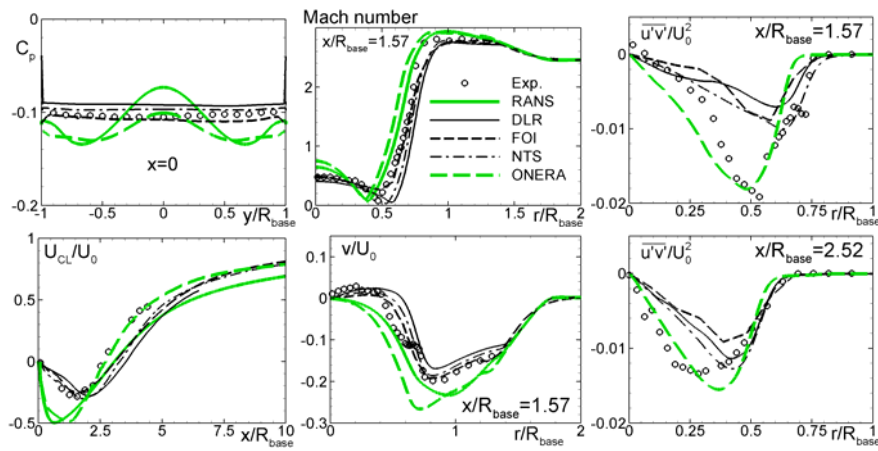


Figure 16 Comparison of performance of turbulence-resolving approaches on the finest available grids with each other and with S-A CC RANS solution. DLR: S-A DES, NTS fine grid; FOI: HYB0, FOI structured grid; NTS: S-A DES, NTS fine grid; ONERA: zonal S-A DES ($C_{DES}=0.40$), ONERA very fine grid

Finally, Fig.16 compares performance of the three considered turbulence-resolving approaches (S-A DES, HYB0, and zonal S-A DES) on the finest available grids with each other and with the best available RANS solution (S-A model with the compressibility correction). It suggests that the standard S-A DES

and HYB0 predictions of DLR, FOI, and NTS are all close to each other, while the zonal DES is apart from these simulations and, as mentioned above, provides for a much better prediction of the shear layer but fails to predict the flow inside the recirculation zone. A reason of the latter deficiency of the zonal DES remains unclear. As already noted, one of possible explanations is the use of the “non-standard” subgrid length-scale definition $\Delta=(\Delta_x \Delta_y \Delta_z)^{1/3}$ and C_{DES} value.

11.5 Conclusions

In the course of DESider a series of simulations of the supersonic base flow is carried out with the use of different modelling approaches (S-A and S-A CC RANS, S-A DES, HYB0, and zonal S-A DES), CFD codes (DLR, FOI, ONERA, and NTS), and grids (unstructured and structured of different size, from 0.9 up to 14 million nodes). Comparison of results of these simulations with each other and with experimental data of Herrin and Dutton (1994) permits to make the following conclusions.

As far as the models performance is concerned, in accordance with the expectations, all the turbulence-resolving approaches turn out to be much more accurate than the S-A RANS, even if used with the compressibility correction, which results in some tangible improvements. However, all these approaches, except for the zonal S-A DES of ONERA, fail to provide accurate representation of the initial region of the separated shear layer. Analysis of the results suggests that this failure is caused by insufficiently fine grids in this region used in the simulations of DLR, FOI, and NTS. On the other hand, inside the recirculation zone, the mean flow predicted by zonal DES on the very fine grid demonstrates a “RANS-like” behaviour and, in particular, fails to reproduce the flat distribution of the base-pressure observed in the experiment, whereas both S-A DES and HYB0 model do this fairly well even with relatively coarse structured grids of about two million nodes. The only conjecture about a reason of this behaviour of the zonal S-A DES we can suggest so far is that it is associated with the use of the non-standard C_{DES} value and of the cube root of cell-volume rather than the maximum grid-spacing as the sub-grid length-scale.

References

- Deck, S. (2005): Numerical Simulation of Transonic Buffet over a Supercritical Airfoil. AIAA Journal, Vol. 43, No. 7, pp. 1556–1566.
- Herrin, J.L., Dutton C.J. (1994): Supersonic Base Flow Experiments in the Near Wake of A Cylindrical Afterbody. AIAA Journal, Vol. 32, No. 1, pp 77-83.
- Peng, S-H. (2005): Hybrid RANS-LES Modeling Based on Zero- and One-Equation Models for Turbulent Flow Simulations. In: Fourth International Symposium on Turbulence and Shear Flow Phenomena – 2005, TSFP-4.
- Simon, F., Deck, S., Guillen, P., Sagaut, P. (????): Reynolds-Averaged Navier–Stokes/Large-Eddy Simulations of Supersonic Base Flow. AIAA Journal, Vol. 44, No. 11, pp. 2578-2590.
- Spalart, P.R. (2000): Trends in Turbulence Treatments, AIAA Paper No. 2000-2306.